JOURNAL OF MATERIALS SCIENCE 30 (1995) 1409–1419

Deformation micromechanics in model carbon fibre-reinforced composites

Part I *The single-fibre pull-out test*

X.H. GU, R.J. YOUNG, R.J. DAY
Manchester Materials Science Centre, UMIST/University of Manchester, Grosvenor Street, Manchester M1 7HS, UK

Raman spectroscopy has been used to study the deformation micromechanics of the single-fibre pull-out test for a carbon fibre/epoxy resin system using surface-treated and untreated versions of the same type of PAN-based fibre. It has been possible to determine the detailed strain distribution along embedded fibres and it has been found that it varies with the level of strain in the fibre outside the resin block. The variation of interfacial shear stress along the fibre/matrix interface has been determined using the balance of forces equilibrium and this has been compared with the single values of interfacial shear strength determined from conventional pull-out analyses. It has been demonstrated that it is possible to identify situations where the interface is well-bonded, partially debonded or fully debonded and also to follow the failure mechanisms in detail. It has been found that the level of interfacial adhesion is better for the surface-treated fibre and that, for the untreated fibre, interfacial failure takes place by the cohesive failure of a weakly-bonded surface skin that appears to be removed by the surface pretreatment process.

1. Introduction

The fibre–matrix interface plays a major role in determining the mechanical performance and structural integrity of fibre-reinforced composites [1, 2]. The significance of the interfacial properties has directed substantial research efforts to both experimental and theoretical characterization of the interface. The single-filament pull-out test has received considerable attention in recent years as a method of measuring the interfacial shear strength (IFSS) [3–6]. There are several advantages to this test. Firstly, it is a direct measure of the quality of the adhesive bond between the fibre and matrix. Secondly, it requires only small amounts of fibre and matrix. Thirdly, the pull-out test is not generally limited by the properties of fibre and matrix. This should be compared with the fragmentation test [7] where the failure strain of the matrix needs to be more than three or four times the failure strain of the fibres to meet the needs of achieving a saturated fragmentation state. The pull-out test can be carried out successfully with both brittle and ductile matrix systems.

In practice, however, the use of the single-filament pull-out test is still controversial. This is because the data analysis for the test is still a matter of some dispute [5, 8]. It is normally assumed that the IFSS is given of the pull-out force divided by the interfacial area. It has been realized in recent years that this ratio only represents an approximate estimate of the IFSS [9]. This is because the interfacial shear stress (ISS) distribution at the interface is not thought to be uniform and in some cases interfacial debonding or matrix yielding will occur locally before the load reaches the pull-out force [10]. In recent studies, mathematical modelling [10, 11] and finite element analyses [12, 13] have been used to try accurately to interpret the experimental results.

Raman spectroscopy has been developed over the past few years as a new technique for strain measurement with high-modulus fibres [14]. It is found for a wide variety of high-performance fibres that the bands in their Raman spectra shift on the application of stress to the fibres [15–19]. Because a laser beam can be focused to a fine point of about 2 μm on a specimen, this band shift can be used to measure directly the strain distribution from point-to-point along a fibre embedded in a transparent matrix [20–23]. In this work, Raman spectroscopy has been used to follow fibre deformation during pull-out tests for a carbon fibre/epoxy resin system. A comparison is also made between the results of conventional pull-out tests and those obtained using Raman spectroscopy.

2. Background

2.1. Elastic stress transfer

The study of load transfer between a fibre and a matrix started with the work of Cox [24], who

0022–2461

analysed the stress transfer around a short embedded fibre in a matrix using shear-lag theory. The basic assumption of the shear-lag analysis is that all the tensile load is carried by the fibre and all the shear loads are carried by the matrix. The fibre and matrix are assumed to be elastic and the bond between the fibre and the matrix is assumed to be perfect. Several groups [25–30] have used Cox's [24] shear-lag principle to predict the stress and strain distributions along an embedded fibre for the pull-out test. Chua and Piggott [27–30] proposed a Cox-type shear-lag model where the strain distribution along the fibre of radius, r_0, and embedded length, L, is given by

$$e = e_f \frac{\sinh[n(L - x)/r_0]}{\sinh(ns)} \quad (1)$$

where x is the distance from the point where the fibre enters the resin block, $s = L/r_0$, e_f is the average strain in the fibre outside the resin and

$$n^2 = \frac{E_m}{E_f(1 + \nu_m)\ln(R/r_0)} \quad (2)$$

where E_f and E_m are the Young's moduli of the fibre and matrix, respectively, ν_m is Poisson's ratio of the matrix and R is the radius of the resin block. Equation 1 predicts that the fibre strain should decay rapidly from the point where the fibre enters the resin block and fall to zero some distance inside the block, as shown schematically in Fig. 1.

The shear stress at the interface can be calculated from the equilibrium of forces exerted on a differential fibre element, of length dx, through the well-known equation [31]

$$\tau = E_f \frac{r_0}{2}\left(\frac{de}{dx}\right) \quad (3)$$

where τ is the interfacial shear stress (ISS) and (de/dx) is the differential of the variation of fibre strain with distance along the fibre. By combining Equations 1 and 3, the interfacial shear stress distribution along the fibre is given by

$$\tau = n\sigma_f \frac{\cosh[n(L - x)/r_0]}{2\sinh(ns)} \quad (4)$$

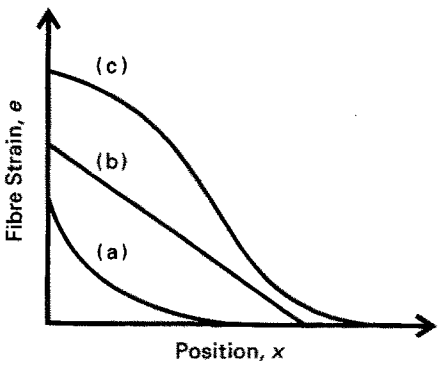

Figure 1 Schematic representation of the distribution of fibre strain inside the resin block for the single-fibre pull-out test showing the effect of different types of stress transfer: (a) fully elastic; (b) fully debonded; (c) partial debonding.

where σ_f is the average tensile stress applied to the fibre outside the resin.

Other workers [12, 13] have employed finite element analysis (FEA) with an appropriate mesh for the pull-out geometry, in order to determine the shear stress distribution along the fibre inside the resin. Their results are generally similar to those of shear-lag analysis. Unfortunately, the FE analyses have primarily been concerned with elastic behaviour. The authors are presently developing FE analyses for pull-out that take into account yielding and inelastic deformation of the matrix resin.

2.2. Debonding

The interfacial shear strength is often evaluated from the load–displacement curve for the pull-out of the fibre from the matrix [32, 33], using the Kelly–Tyson pull-out model which assumes a constant shear stress along the fibre [34]. The model was formulated originally for a matrix undergoing shear yielding at the fibre/matrix interface but it is also appropriate for frictional pull-out with a debonded interface [10]. The interfacial shear strength (IFSS), τ_i, is given by

$$\tau_i = \frac{F_d}{2\pi r_0 L} \quad (5)$$

where F_d is the critical debonding force. A constant shear stress at the interface implies through Equation 3 that the fibre strain in the embedded region should decrease linearly from the point where the fibre enters the resin, as shown schematically in Fig. 1. This approach, however, is very simplistic and it is anticipated that, in reality, the behaviour may be more complicated [33, 36] due to factors such as stress concentrations present at the fibre ends [37], a shrinkage pressure developed at the interface on curing or cooling of the matrix, or if there is an interaction of the stress fields between adjacent fibres [38].

2.3. Partial debonding

In many real pull-out tests it is likely that the situation will be more complicated than those described above. Several workers [10, 11] have considered the possibility of debonding from the point where the fibre enters the resin for some distance along the fibre, such that over this region there is frictional stress transfer. It is then assumed that there is good bonding along the remainder of the fibre with elastic stress transfer. The result of this behaviour upon the distribution of strain within the embedded fibre is shown in Fig. 1 where it can be seen that the strain distribution has a characteristic sigmoidal shape [10, 11].

3. Experimental procedure

3.1. Materials

Two kinds of carbon fibre were used in this study, HM-40 and HMS-40 high-modulus PAN-based carbon fibres both supplied by Akzo. Both fibres were sized but the fibre HM-40 was not surface treated

whereas HMS-40 had been surface pretreated. The reason for choosing the high-modulus carbon fibres is that they have better-defined Raman spectra than the lower modulus fibres [39]. The carbon fibres were washed three times in acetone (at room temperature) to remove the sizing agent, and then dried in air.

The epoxy resin used in the experiment was Ciba–Geigy Araldite LY5052 resin (100 parts by weight) and HY5052 hardener (36 parts by weight), cured at room temperature (22 ± 2 °C) for seven days.

3.2. Scanning electron microscopy (SEM)

A Philips 525 SEM was used to study the surface morphology of the carbon fibres using an accelerating voltage of 20 kV. The carbon fibres were washed in acetone and mounted on the sample stage without coating. A 2160 lines/mm mesh was used to calibrate the magnification of the SEM. The diameter of carbon fibres was measured with the sample at the eucentric height. The average fibre diameters were determined using more than 40 samples of each type of carbon fibre.

3.3. Mechanical testing

An Instron 1121 universal testing machine was used to determine the mechanical properties of the carbon fibres. Individual fibres were mounted on a 50 mm gauge length paper frame using Ciba–Geigy heavy duty epoxy adhesive (slow-setting and room temperature curing). The frames were then placed in the spring-loaded jaws of the Instron and both edges of the frame were cut before the testing. The testing was carried out using a crosshead speed of 0.5 mm min^{-1}, at a temperature of 23 ± 1°C and with a relative humidity of 50 % ± 2%.

3.4. Raman spectroscopy

Raman spectra were obtained using the 448 nm line of argon-ion laser operated at a power level of about 7 mW (< 1 mW on the sample). A Raman microprobe system was used which is based on a modified Nikon optical microscope and a Spex 1403 double monochromator. A × 40 objective lens and a spatial filter with a 400 μm pin hole were used to collect the 180° backscattered light. A liquid-nitrogen cooled highly sensitive Spex Charge-Coupled Device (CCD) camera was employed as a photon counting system to record the Raman spectra. The laser polarization direction was always parallel to the axis of both the free-standing carbon fibres and the fibres in the composites. The intensity of the laser beam on the fibre was less than 1 mW and the spot size was about 4 μm. The Spex DM3000s software was used for data collection and analysis.

3.5. Preparation of pull-out specimens

It is difficult to prepare pull-out specimens with fine, brittle fibres and for high bond-strength systems, such as carbon fibre/epoxy composites. The most common method is to dip one end of a filament into a pot of uncured resin and hold it in position until the curing has finished. There are difficulties in handling the fine filaments and controlling the length of filaments dipped in the resin. A number of variants have, therefore, been proposed, including threading the fibre through a resin film supported by a small hole in a thin metal stock or through a slit between steel blades [40], or the resin being cured as a biconcave button on a bath of mercury with the filament crossing at the exact centre of the button [41, 42]. Owing to the shape of the button, the thickness can be made very small so that a short embedded length could be obtained. Unfortunately these kinds of specimens are not suitable for use in the Raman spectroscopy experiment because the geometry of the specimens makes it difficult to focus the laser beam perpendicular to the fibre surface in the resin. Marshall and Price [43] designed another microcomposite involving the immersion of the fibre in a small volume of the resin. This makes it possible to observe the events which occur at the fibre/matrix interface such as interfacial debonding and fibre pull-out. A problem with this method is that the embedded length is difficult to control due to the effect of capillarity.

In the present study a special technique was developed to prepare the pull-out specimens (Fig. 2). The process was as follows. Firstly, a paper card frame was placed on the micrometer deformation stage. A small piece of a glass cover slide was fixed to one end of the frame, and then a single carbon-fibre filament was mounted in position using adhesive tape with one end on the cover slide and other end on the moving stage of the micrometer (as shown in Fig. 2). Secondly, a small drop of the uncured resin was put on the filament at the edge of the cover slide and the fibre was cut above the resin drop (point A, Fig. 2). Thirdly, during observation in the microscope, the stage of the micrometer was to pull the fibre out of the uncured

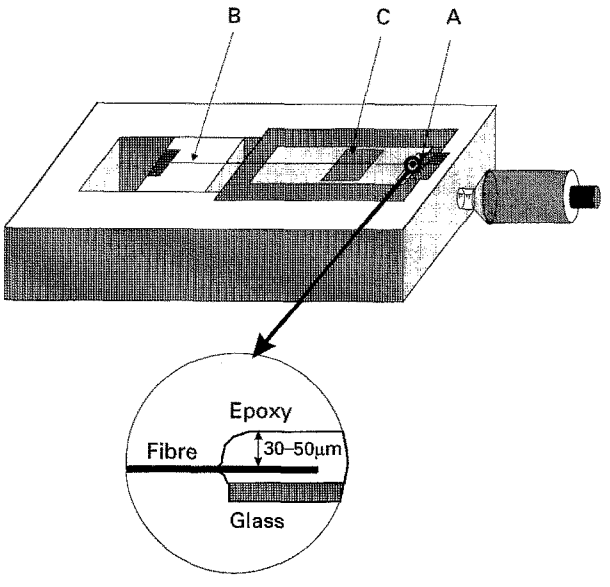

Figure 2 Schematic diagram of the deformation rig used for pull-out specimen preparation, single-fibre Raman deformation and Raman pull-out tests.

resin until the desired embedded length was achieved. Finally, the fibre was mounted on the other end of the frame and the fibre was cut at point B. The function of stage C is to hold the fibre in the correct position during the specimen curing process. At this point the specimen (including stage C) could be removed for curing and the micrometer stage could be used for the preparation of another specimen. The advantages of this method are that the embedded length could be controlled precisely and capillarity could be prevented by having a meniscus at the edge of the cover slide.

3.6. Conventional pull-out testing

The mechanical pull-out tests were performed under similar conditions as were used for the single-fibre testing (Section 3.3). An Instron 1121 Universal Testing Machine fitted with a 5 N load cell was used. The specimens were prepared as shown in Fig. 2 and were mounted between two spring-loaded jaws. The paper frames edges were then cut and the pull-out tests were conducted at crosshead speed of 0.05 mm min^{-1}.

3.7. Raman single-fibre deformation and pull-out

The micrometer straining rig shown schematically in Fig. 2 was also used for the deformation of free-standing non-embedded carbon fibres. Single filaments were fixed between aluminium foil tabs which were glued on the two blocks of the strain rig using cyanoacrylate adhesive. A gauge length 20 mm was used. The filament was deformed by displacing one block of the strain rig using a micrometer which could be read to $\pm$ 0.005 mm. This allowed a precision of the order of $\pm$ 0.025% for strain measurement. Raman spectra of these free-standing carbon fibres were obtained during the deformation.

The pull-out tests were also carried out using the micrometer-controlled straining rig. The stages C (Fig. 2) were removed before the specimens were put on the micrometer stages. Both ends of paper frame were fixed on the aluminium blocks using cyanoacrylate adhesive. The frame edges were cut before the test. The whole fibre-embedded area was scanned at different strain levels and Raman spectra were obtained from the fibre at 10 μm intervals both outside and inside the resin drops.

4. Results and discussion

4.1. Fibre structure and properties

Scanning electron micrographs of the surfaces of the carbon fibres are shown in the Fig. 3. It can be seen that both fibres have surface grooves parallel to the fibre axis but that there is no significant difference between the HM-40 and HMS-40 carbon fibres from SEM observation.

The Raman spectra of the two types of fibre are shown in Fig. 4. It is known [44] that in disordered carbon the G line (at 1580 cm^{-1}) is broadened and blue-shifted, the D line (at 1360 cm^{-1}, which is believed to result from structural imperfections) is

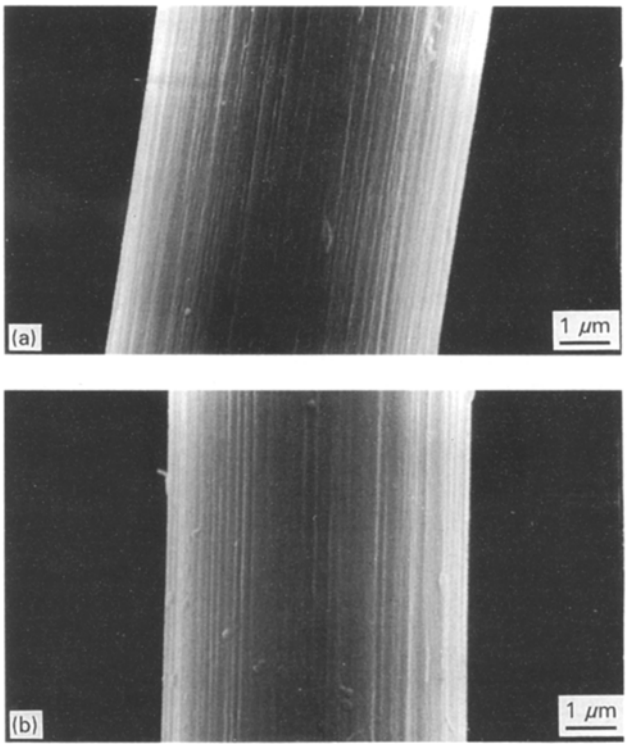

Figure 3 Scanning electron micrographs of the carbon fibres: (a) HM-40, and (b) HMS-40.

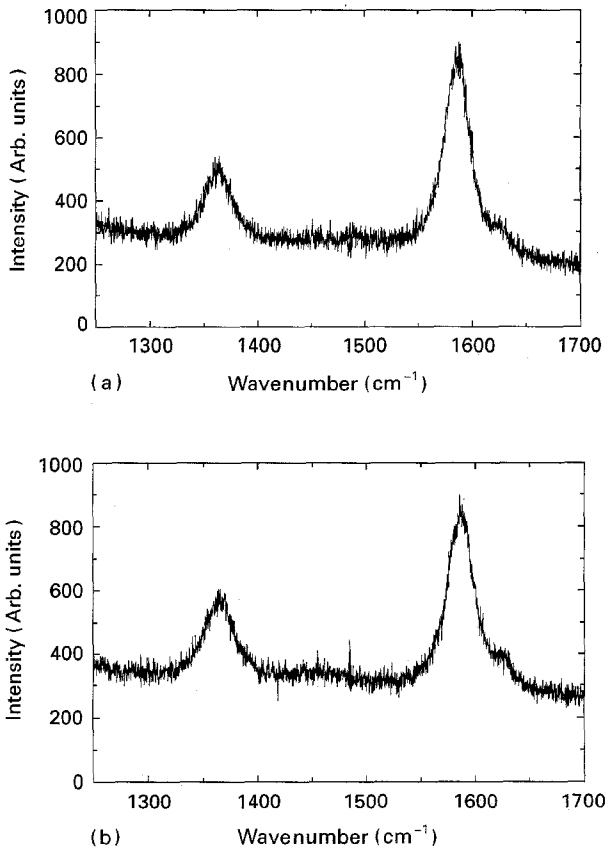

Figure 4 Raman spectra of the carbon fibres in the range 1200–1700 cm^{-1}: (a) HM-40, and (b) HMS-40.

stronger compared to more ordered carbon. From the comparison of the intensities of the two Raman bands (I_G/I_D) for the two systems, the HM-40 fibre has a higher value (2.42) than the HMS-40 carbon fibre (2.16). Because the laser beam only penetrates less

than 100 nm below the fibre surface [45], this means the crystalline structure of the HMS-40 carbon fibre structure is not as perfect as that for the HM-40 fibre, due probably to the surface treatment given to HMS-40.

The fibre diameters measured using SEM and the mechanical testing results are shown in Table I. It can be seen that after surface treatment the fibre diameter decreased, probably due to the removal of surface layers of the fibre. It is generally found that the surface treatment does not have a strong effect upon the mechanical properties of the fibres except for a slight reduction in fibre strength, σ_f^* [46].

TABLE I Mechanical properties of HM-40 and HMS-40 carbon fibres

	HM-40	HMS-40
Diameter d(μm)	7.22 ± 0.34	6.73 ± 0.21
Tensile strength σ_f^*(GPa)	2.64 ± 0.43	2.56 ± 0.27
Strain at failure, e_f^*(%)	0.78 ± 0.12	0.74 ± 0.07
Modulus, E(GPa)	338 ± 31	350 ± 23

TABLE II Mechanical properties of the epoxy resin

Tensile yield strength (MPa)	68 ± 9
Elongation at break (%)	1.9 ± 0.4
Modulus (GPa)	3.45 ± 0.1
Compressive yield stress (MPa)	109 ± 8
Shear yield strength (MPa)	41.8 ± 2.0

The mechanical properties of epoxy resin were also investigated and the results are shown in Table II. The shear yield strength, τ_y was derived from the compressive and tensile yield strengths, σ_{yc} and σ_{yt}, using [14]

$$\tau_y = \frac{\sigma_{yc}\sigma_{yt}}{\sigma_{yc} + \sigma_{yt}} \quad (6)$$

4.2. Raman deformation of carbon fibres

The second-order Raman bands of the carbon fibres [47] shown in Fig. 5 were chosen to monitor the strain in the fibres in the resin. The merit of using the second-order Raman band is that it is less influenced by the Raman spectrum of epoxy resin compared to the first-order carbon-fibre Raman bands because the epoxy resin used in the experiment has several Raman bands between 1250 and 1610 cm^{-1}. These tend to overlap with first-order bands of carbon fibres and make it difficult to measure accurately the Raman band positions and shifts. Also the rate of shift of the second-order band with strain of the fibre is larger than that of the first-order bands [47].

Fig. 6a and b show the dependence of the position of the Raman bands at different fibre strain levels. It can be seen that there is an approximately linear decrease in the Raman peak position with the increasing strain, which is about 25–28 cm^{-1} %/strain, up to

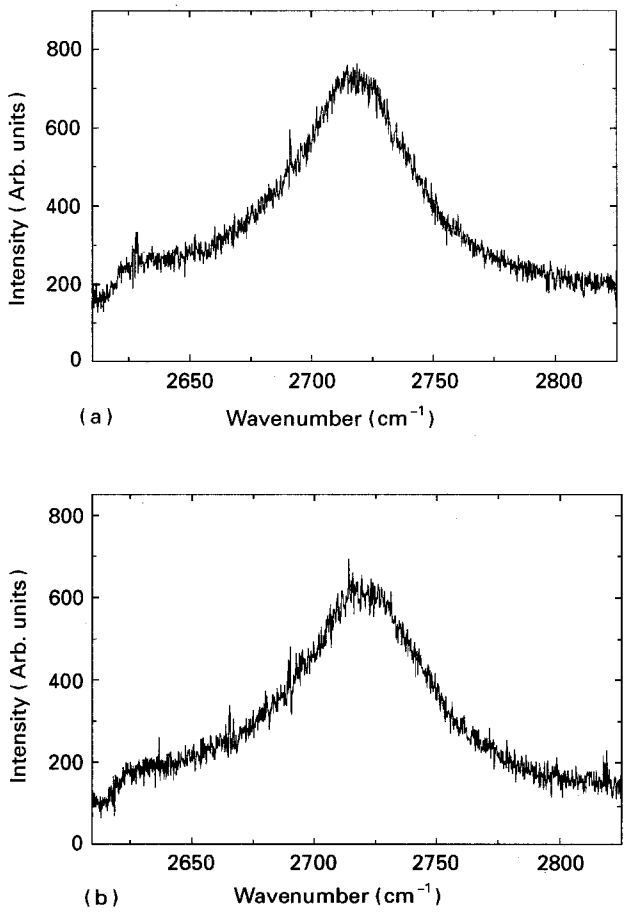

Figure 5 Raman spectra of the carbon fibres in the range 2610–2825 cm^{-1} showing the second-order band: (a) HM-40 and (b) HMS-40.

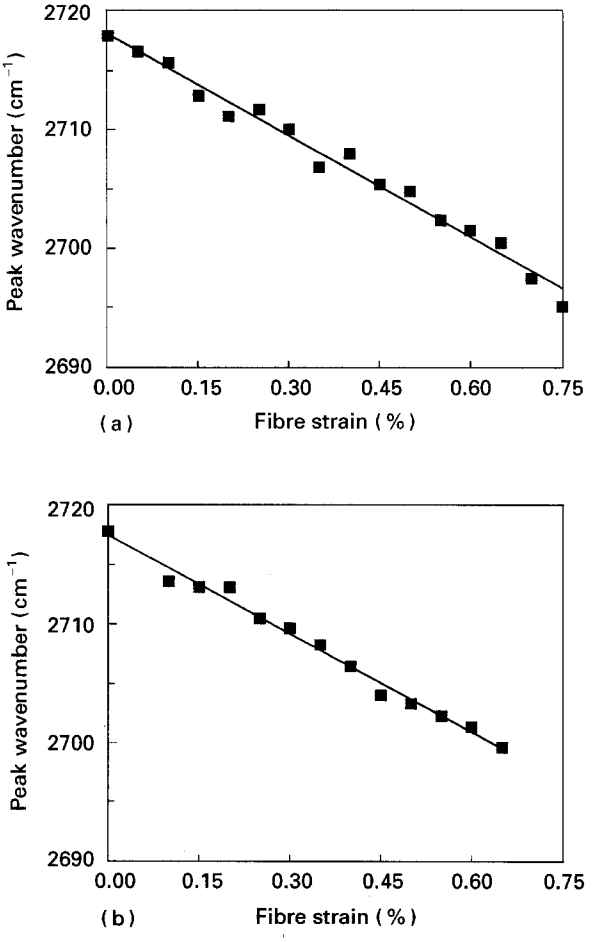

Figure 6 Dependence of the peak positions of the second-order Raman bands upon strain for (a) HM-40, and (b) HMS-40.

fibre failure. There was no distinguishable difference between the Raman deformation behaviour of the HM-40 and the HMS-40 carbon fibres.

4.3. Conventional pull-out testing

Fig. 7 is a typical load–displacement curve obtained during pull-out tests for the two systems used. The embedded lengths of the specimen were between 60 and 140 μm (a longer embedded length led to fibre failure instead of fibre pull-out). From the pull-out studies reported before [48], this kind of curve is typical of a system undergoing a catastrophic type of failure process. This means the system has a strongly bonded interface and the strain energy stored in the system is so high that pull-out immediately follows interfacial failure.

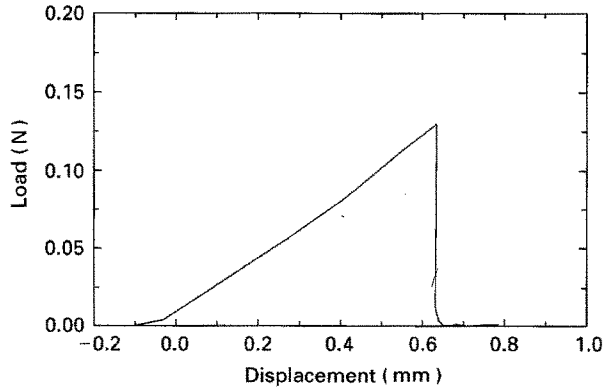

Figure 7 Typical load–displacement curve for the single-fibre pull-out test.

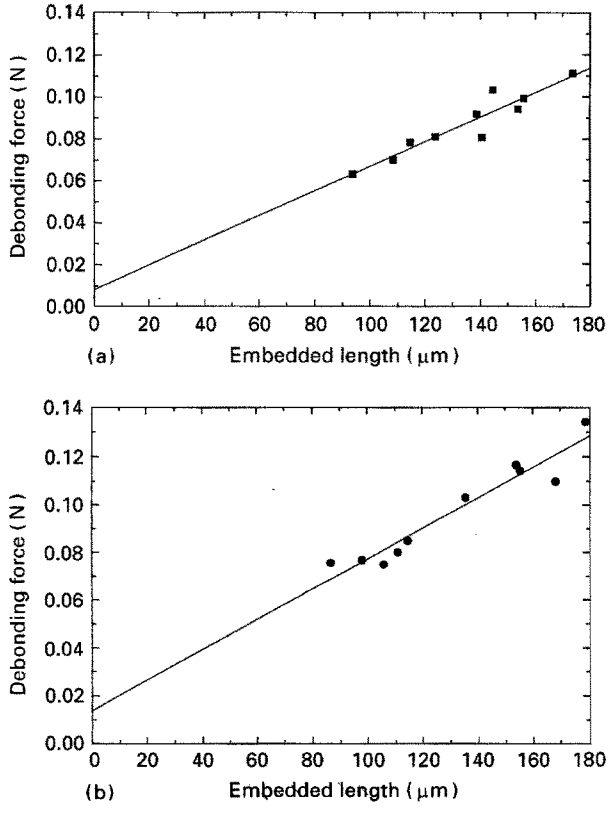

Figure 8 Variation of debonding force with embedded fibre length for pull-out tests with (a)HM-40, and (b) HMS-40.

Fig. 8 shows the variation of the debonding force, F_d, with embedded length, L, for the two systems. Because the systems have comparatively high bond strengths and low fibre strengths, it was difficult to obtain data over a wide range of embedded lengths. It can be seen that the data are rather scattered but both sets of data fall on straight lines, as predicted by Equation 5. It should be pointed out, however, that the data extrapolate to finite values of debonding force for zero embedded length – a point also noted by previous workers [10]. This is developed in Fig. 9 which shows the variation of the IFSS with embedded length for the two fibre systems. It can be seen that, for both systems, the apparent interfacial shear strength increases as the embedded length decreases.

The influence of the embedded length upon pull-out behaviour has been considered in several studies [48]. According to Equation 5, there should be a linear increase of the debonding force, F_d, with embedded length, L. In fact, this will only be the case when plastic flow of the matrix takes place near to the fibre/matrix interface or if there is frictional slip at the interface. Two other types of behaviour have been reported. In an ideally elastic system, F_d will increase with L following a curve, the slope of which reduces progressively up to an asymptotic value for large values of L. Another situation was observed by Piggott and Andison [49] for a carbon fibre/epoxy resin system with a low level of resin shrinkage, where

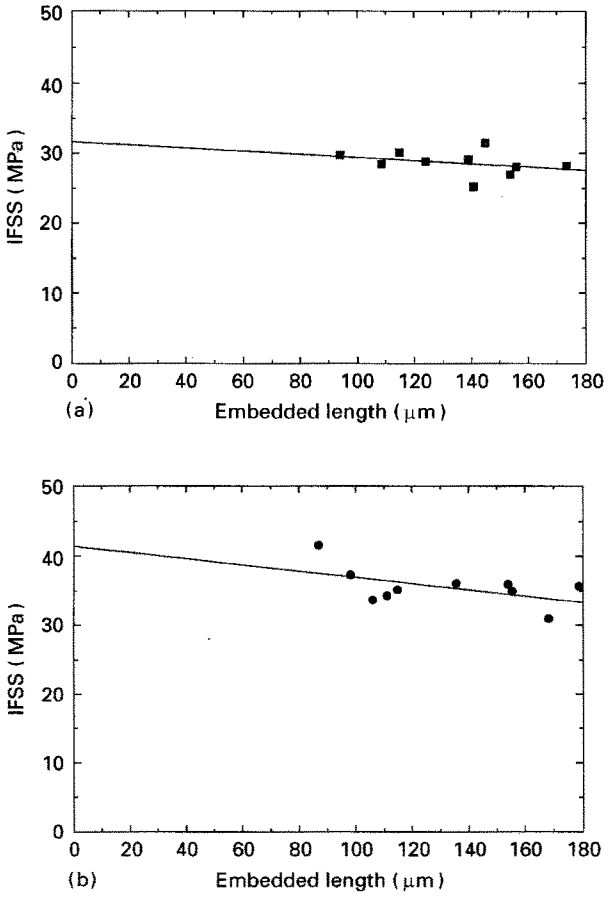

Figure 9 Variation of interfacial shear strength (IFSS), calculated using Equation 5, with embedded fibre length for pull-out tests with (a) HM-40, and (b) HMS-40.

F_d was apparently independent of the embedded length.

From Fig. 8, it can be seen that for the HM-40 and HMS-40 carbon fibre/epoxy systems, Equation 5 is not obeyed and the data show some characteristics of an elastic system [48]. Further light is shed on this behaviour in the Raman study described next, where it is found that there is a complicated stress distribution in the fibres in the pull-out specimens.

4.4. Raman pull-out tests

Raman spectroscopy was used to scan the embedded fibres during the pull-out process and determine the point-to-point variation of fibre strain. Fig. 10 shows the strain profiles (determined from Raman bands shifts) of short ($\sim 100\,\mu m$) embedded HM-40 and HMS-40 fibres at different levels of applied fibre strain, e_f. The curves are Boltzmann functions fitted to the experimental points in Fig. 10 and have no theoretical justification.

At low applied strains, both systems show similar fibre strain profiles in the embedded regions. There is a sharp decrease in strain where the fibre enters the resin and the strain falls to zero for $x < 50\,\mu m$. As the fibre strain, e_f, is increased above 0.3% strain the fibre strain profiles in the resin for two systems show different patterns of behaviour. For the HM-40 system (Fig. 10a) the strain decreases approximately linearly with position, x. In contrast, the HMS-40 system (Fig. 10b) has a different strain profile at higher fibre strain levels. There is still a rapid decrease in strain after the fibre enters the resin but the curve shifts to the right with increasing applied strain.

For the specimens with longer embedded fibre lengths (Fig. 11), the differences in the pull-out process for the two systems at high strain is more apparent. In the case of the untreated HM-40 fibre (Fig. 11a) the decrease in fibre strain becomes virtually linear but it is noticeably sigmoidal at higher strains for the HMS-40 fibre (Fig. 11b).

4.5. Deformation micromechanics

It is possible to follow the deformation micromechanics of the fibre/matrix interface from the strain distribution profiles in Fig. 10 and 11. At low levels of fibre strain ($e < 0.3\%$) there is a rapid decrease in strain from the point where the fibre enters the resin droplet for both types of fibre and both embedded fibre lengths. This is the type of behaviour expected for the case of elastic stress transfer (Equation 1 and Fig. 1). At higher levels of fibre strain, the behaviour of the two types of fibres differs. In the case of the HM-40

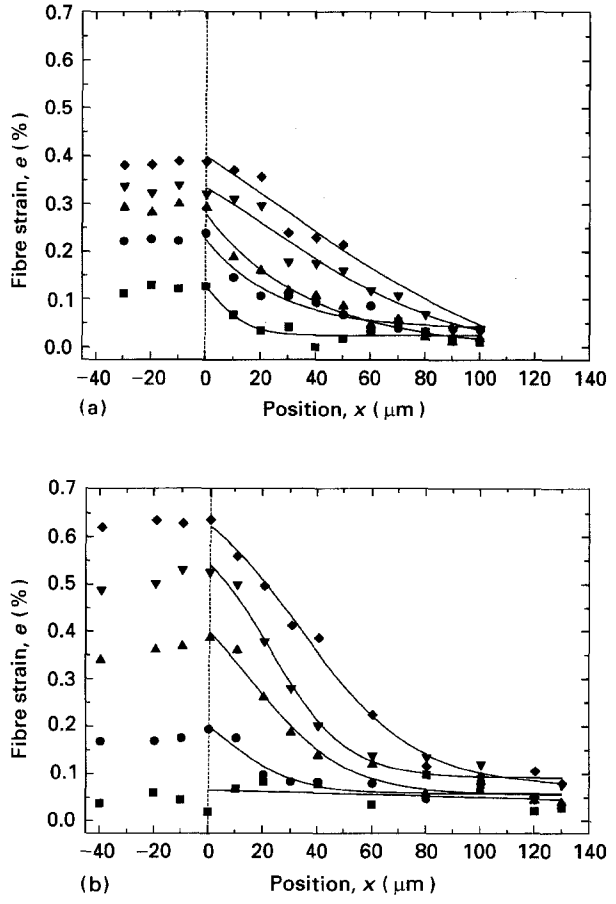

Figure 10 Variation of fibre strain with position inside the resin (positive values) during pull-out using different levels of applied fibre strain, e_f, for short embedded lengths: (a) HM-40 and (b) HMS-40. e_f: (a) (■) 0.12%, (●) 0.24%, (▲) 0.29%, (▼) 0.32%, (◆) 0.38%; (b) (■) 0.02%, (●) 0.19%, (▲) 0.38%, (▼) 0.52%, (◆) 0.64%.

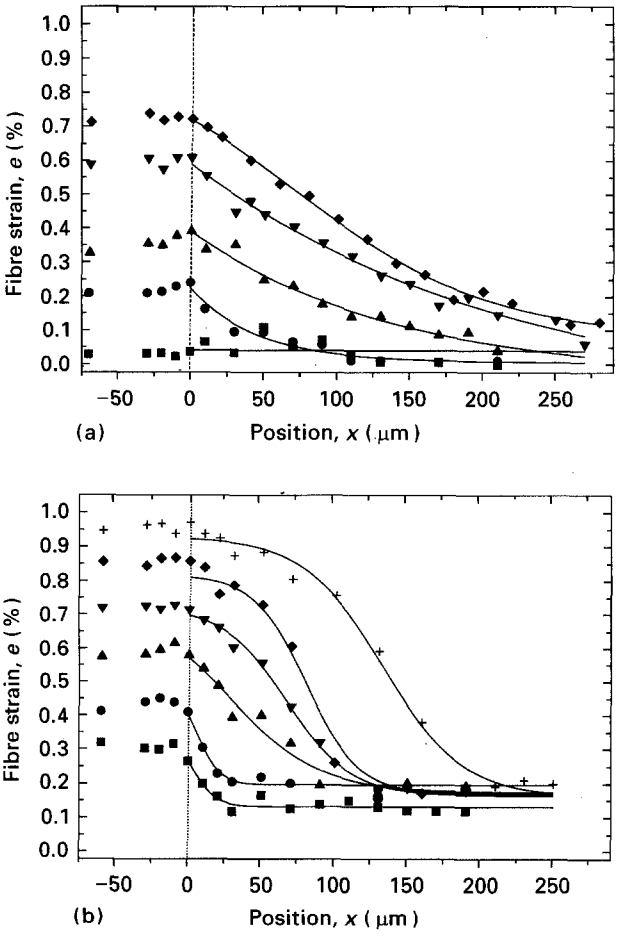

Figure 11 Variation of fibre strain with position inside the resin (positive values) during pull-out using different levels of applied fibre strain, e_f, for long embedded lengths: (a) HM-40, and (b) HMS-40. e_f: (a) (■) 0.03%, (●) 0.24%, (▲) 0.39%, (▼) 0.61%, (◆) 0.72%; (b) (■) 0.26%, (●) 0.41%, (▲) 0.57%, (▼) 0.71%, (◆) 0.85%, (+) 0.97%.

fibres (Figs 10a and 11a) the rate of decrease of strain becomes lower and the decay of strain at higher levels of e becoming approximately linear. This type of behaviour is characteristic of debonding taking place with frictional pull-out (Fig. 1). The behaviour of the HMS-40 fibres at higher levels of strain ($e_f > 0.4\%$) is rather different (Figs 10b and 11b). The curves take on a markedly sigmoidal shape, particularly for the longer embedded length (Fig. 11b). This is indicative of failure taking place through a partial debonding mechanism (Fig. 1) with a debonded region starting at the point where the fibre enters the resin and then moving along the fibre as the strain is increased [10, 11].

The curves fitted to the strain distributions in Figs 10 and 11 have been converted to the ISS profiles in Figs 12 and 13 using the balance of forces approximation (Equation 3). Several interesting points can be seen from the ISS profiles that confirm the failure mechanisms suggested above. At low levels of strain ($e_f < 0.3\%$) the ISS decreases rapidly with position along the fibre, x, for both types of fibres and both embedded lengths as predicted by the elastic stress transfer theory (Equation 4). The high-strain behaviour is again different for the two types of fibre. In the case of the HM-40 fibres, the ISS becomes approximately constant at about 10–20 MPa, whereas for the HMS-40 fibres the ISS peaks at about 40–50 MPa and the peak position moves along the fibre, away from the point where the fibre enters the resin, as the strain is increased.

It is possible to obtain a further insight into the failure processes from Fig. 14 which shows the relationship between the peak value of ISS, τ_{max}, during the pull-out process and the strain in the fibre outside

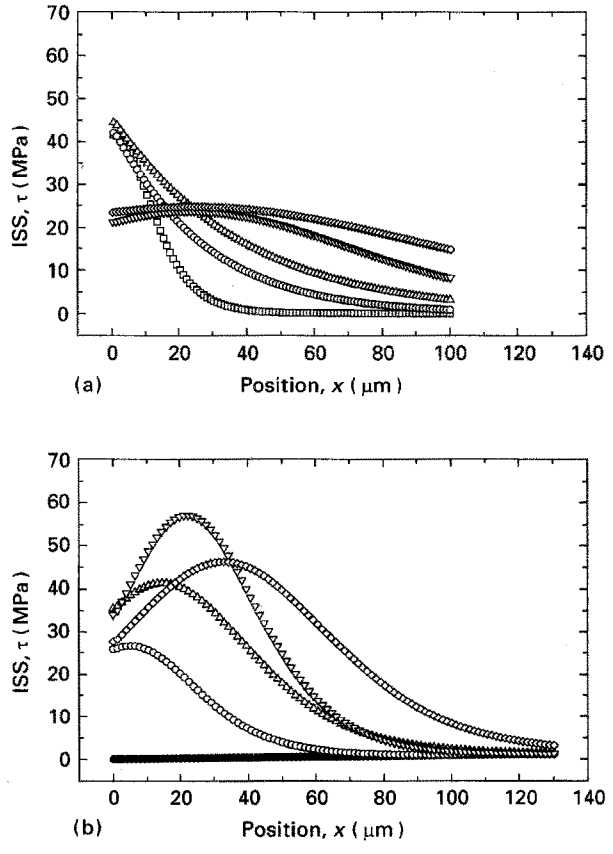

Figure 12 Variation of interfacial shear stress, τ, derived using Equation 3, with position inside the resin during pull-out using the data from Fig. 10 for different levels of applied fibre strain, e_f: (a) HM-40, and (b) HMS-40. e_f: (a) (□) 0.12%, (○) 0.24%, (△) 0.29%, (▽) 0.32%, (◇) 0.38%; (b) (●) 0.02%, (○) 0.19%, (△) 0.38%, (▽) 0.52%, (◇) 0.64%.

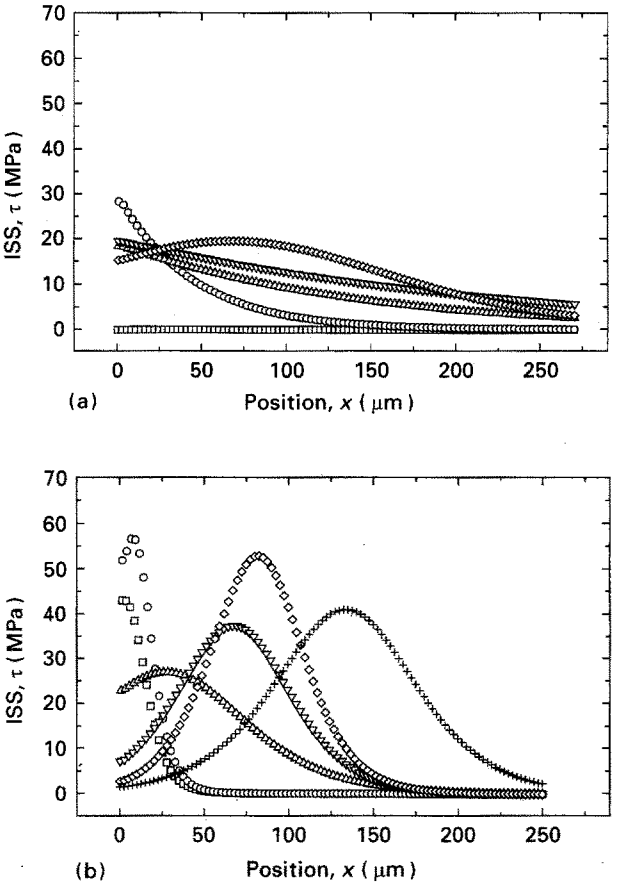

Figure 13 Variation of interfacial shear stress, τ, derived using Equation 3, with position inside the resin during pull-out using the data from Fig. 11 for different levels of applied fibre strain, e_f: (a) HM-40, and (b) HMS-40. e_f: (a) (□) 0.03%, (○) 0.24%, (△) 0.39%, (▽) 0.61%, (◇) 0.72%; (b) (□) 0.26%, (○) 0.41%, (△) 0.57%, (▽) 0.71%, (◇) 0.85%, (+) 0.97%.

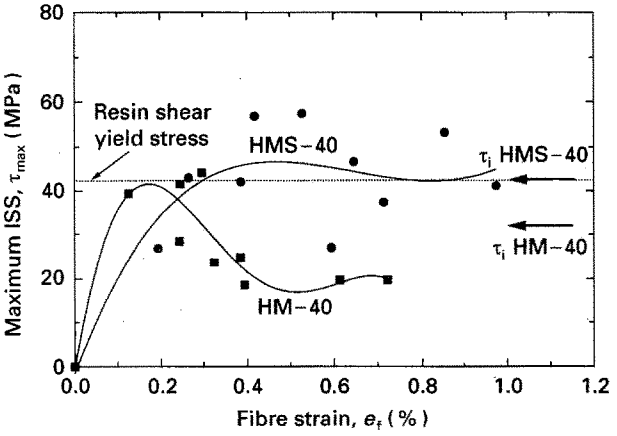

Figure 14 Maximum values of interfacial shear stress, τ_{max}, as a function of fibre strain, e_f, derived from the data in Figs 12 and 13 for the two types of fibre. The values of interfacial shear strength, τ_i, determined from conventional pull-out testing (Figs 8 and 9) are also indicated. (■) HM-40, (●) HMS-40.

the droplet. The values of IFSS, τ_i, determined from the conventional pull-out analysis (Figs 8 and 9 for $L \rightarrow 0$) and the shear yield stress of the matrix resin, τ_y, are also indicated in the figure. The curves are polynomial fits to the experimental data points. Although there is some scatter in the Raman data, several points emerge. In the case of the HM-40 fibre, τ_{max} reaches the shear yield stress of the matrix at low strain but then falls away to about 20 MPa for $e_f > 0.4\%$. It appears, therefore, that in this case the shear yield stress of the resin may be achieved at the interface at low strains but at higher strains the interface fails and frictional pull-out occurs. In contrast, for the HMS-40 system, interfacial failure appears to occur when the peak ISS, τ_{max}, is around the matrix shear yield strength for all levels of fibre strain, e_f. It appears, therefore, that interfacial failure in the HMS-40 system takes place initially through shear yielding of epoxy resin matrix at the fibre/matrix interface. However, the full distributions of ISS in Figs 12b and 13b showed that the ISS decreases following yielding, indicating that debonding follows the yield process even for the relatively well-bonded HMS-40 fibre. This confirms that the HMS-40 and HM-40 systems appear to have different interfacial failure modes.

An important point to consider at this stage is the relationship between the values of τ_{max} in Fig. 14 and the values of apparent IFSS, τ_i, determined using the conventional pull-out analysis. The value of τ_i for the HMS-40 fibre system is 41 $\pm$ 2 MPa which is exactly the same as the shear yield stress of the resin matrix. Because the Raman analysis suggests that failure takes place for this system through shear yielding, it is clear that in the case of the well-bonded HMS-40 fibre the value of IFSS is controlled by matrix shear yielding at the fibre/matrix interface. In the case of the HM-40 fibre, the value of τ_i is 32 $\pm$ 2 MPa which is lower than the shear yield stress of the matrix resin. It can be seen from Fig. 14 that at high strains the value of τ_{max} decreases with strain due to interfacial debonding. This is also reflected in the measured value of τ_i and it is clear that the results of the conventional and Raman analyses can be reconciled for the two systems.

Attempts to fit the experimental distributions of fibre strain and ISS quantitatively to the models described in Section 2 have not met with much success. One of the reasons for this is the presence of a meniscus at the point where the fibre enters the resin. A typical meniscus in one of the specimens is shown in Fig. 15 and it is very difficult to model the stress distributions for such a geometry using analytical models. This can best be done using finite element methods [12, 13].

4.6. Failure modes

Fig. 16 shows a set of transmission optical micrographs obtained between two crossed polars for the HM-40/epoxy systems obtained during a pull-out experiment. It can be seen that a bright birefringent sheath developed from where the fibre enters the resin to cover the whole interfacial area with the increasing pull-out force. This birefringence is believed to be

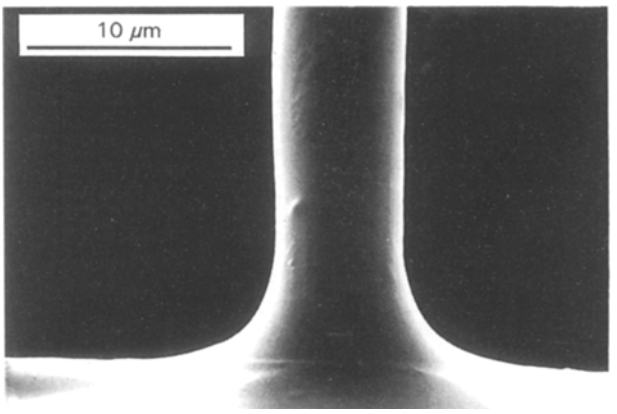

Figure 15 A typical meniscus in one of the specimens.

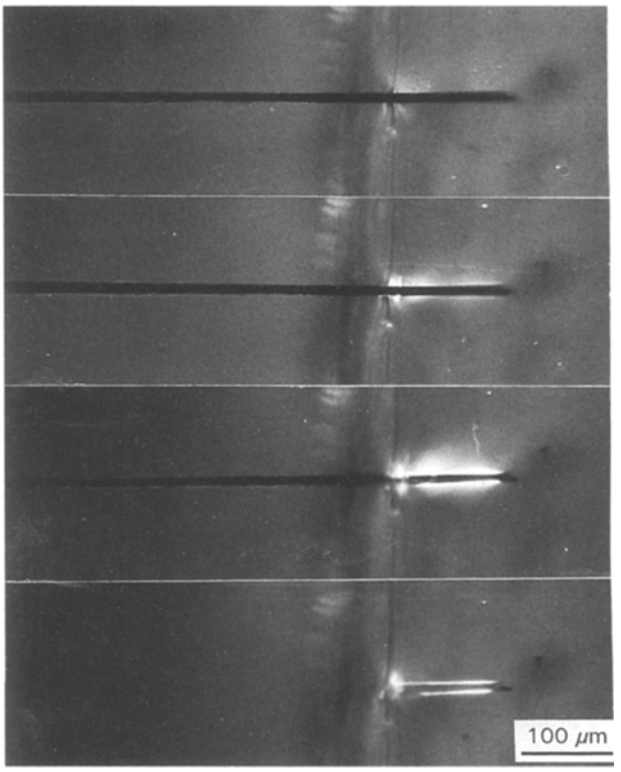

Figure 16 Set of transmission optical micrographs obtained using polarized light for an HM-40 pull-out specimen with an embedded length of about 120 μm: (a) undeformed, (b) low strain level, (c) high strain level, and (d) after pull-out.

caused by the matrix deformation near the interface and it can be seen that a birefringent sheath is left in the resin after pull-out. It was found that for the HMS-40 system a brighter and clearer birefringent sheath pattern was left after the fibre pulled out than for the HM-40 system. This confirms that matrix yielding takes place during the pull-out process and that yielding is more extensive for the HMS-40 system.

An unusual phenomenon was also observed during the Raman pull-out analysis. After the fibre was pulled out from the matrix a cylindrical cavity was left in the resin. When a Raman spectrum was obtained from the walls of the cavity, it still showed a carbon Raman band for the HM-40 system (Fig. 17a). It is known that the Raman spectra for carbon fibres are only obtained from the surface of the fibre, less than 100 nm thick

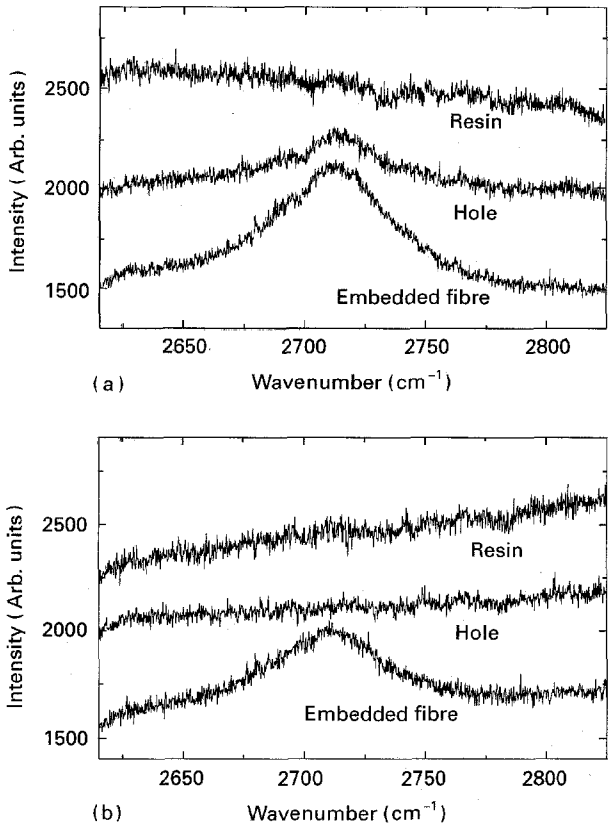

Figure 17 Raman spectra in the range 2160–2825 cm^{-1} of the embedded fibres, the resin matrix and the hole for (a) the HM-40, and (b) the HMS-40 pull-out specimens.

[45]. Although the band is less well-defined than that for the fibre in the resin, it clearly means a thin layer of carbon of the order of 100 nm thick (most probably a skin sheath of carbon fibre) is left lining the cavity. This phenomenon was not found in the HMS-40 system (Fig. 17b). This confirms that the two systems may have different failure modes. It is known that interfacial failure can occur by at least three different processes: (a) cohesive failure of resin near to the interface; (b) adhesive failure at the interface; (c) cohesive failure of fibre near to the interface [50]. From the discussions outlined above it appears that for the HM-40 system, the interfacial failure mode is most probably cohesive failure of the fibre. In contrast, for the HMS-40 system, failure eventually occurs by adhesive failure or cohesive failure of the matrix.

The different failure mechanisms give an explanation as to why the strain profiles for the two systems seen in Figs 10 and 11 are different. In particular, it appears that the shear stress at the interface leads to the removal of an apparently weakly bonded fibre skin for the untreated HM-40 fibre but to shear yielding of the matrix for the surface-treated HMS-40 fibre with the fibre remaining intact. It may be that the most important aspect of the surface pretreatment given to the HMS-40 fibre is simply to remove a weak surface skin rather than any sophisticated change to the surface chemistry of the fibre [35].

5. Conclusion

It has been demonstrated that because the stress distribution at interface is non-uniform and changes during the pull-out process, the IFSS measured using conventional methods only represents an apparent average value.

Although it is difficult to detect from the load–displacement curves of conventional tests, fibre pull-out is a step-wise process when the embedded length is long enough, and it is mainly caused by a region of local interfacial failure moving along the fibre/matrix interface.

The two systems investigated in this present study were found to undergo different failure modes. Raman spectroscopy has proved to be a very useful method of analysing the failure mechanisms for the pull-out test and, in particular, it has been possible to use the technique to detect cohesive failure of the untreated fibres.

Finally, it has been suggested that the maximum interfacial shear strength, τ_{max}, determined using Raman spectroscopy may be the best parameter to characterize the properties of the fibre/matrix interface during the pull-out test.

Acknowledgements

This research is part of a large programme supported by the SERC through a research grant. R.J.Y. is grateful to the Royal Society for support in the form of the Wolfson Research Professorship in Materials Science. X.G. thanks the British Council for financial support and R.J.D. acknowledges the support of T&N Technology for his lectureship in Composites Technology.

References

1. A. T. DIBENEDETTO and L. NICOLAIS, in "Advances in Composite Materials" edited by G. Piatti (Applied Science, London, 1978) pp. 153–81.
2. L. T. DRZAL, in "Advances in Polymer Science 75–Epoxy Resins and Composites II," edited by K. Dusek (Springer, Berlin, Heidelburg, 1986) pp. 3–30.
3. M. J. PITKETHLY and J. B. DOBLE, in "Interfacial Phenomena in Composite Materials '89", edited by F. R. Jones (Butterworth, London, 1989) pp. 35–43.
4. B. MILLER, U. GAUR and D. E. HIRT, *Compos. Sci. Technol.* **42** (1991) 207.
5. K. R. JIANG and L. S. PENN, *ibid.* **45** (1992) 89.
6. S. F. FU, B. L. ZHOU, X. CHEN, G. H. HE and C. W. LUNG, *Composites* **24** (1993) 5.
7. A. T. DIBENEDETTO, *Compos. Sci. Technol.* **42** (1991) 103.
8. J. P. FAVRE, in "Interfacial Phenomena in Composite Materials '89", edited by F. R. Jones (Butterworth, London, 1989) pp. 7–12.
9. R. J. GRAY, *J. Mater. Sci.* **19** (1984) 861.
10. M. R. PIGGOTT, *Compos. Sci. Technol.* **42** (1991) 57.
11. Z.-F. LI and D. T. GRUBB, *J. Mater. Sci.* **29** (1994) 189.
12. C. MAROTZKE, in "Developments in the Science and Technology of Composite Materials", edited by A. R. Bunsell, A. Kelly and A. Massiah (Woodhead, Cambridge, 1993) p. 281.
13. R. J. DAY, "2nd International Conference on Deformation and Fracture of Composites", UMIST, Manchester (Institute of Materials, London, 1993) p. 23/1.
14. R. J. YOUNG, "Polymer Surfaces and Interfaces II" (Wiley, Chichester, 1992) Ch. 6.
15. R. J. DAY, I. M. ROBINSON, M. ZAKIKHANI and R. J. YOUNG, *Polymer* **28** (1987) 1833.
16. X. YANG, X. HU, R. J. DAY and R. J. YOUNG, *J. Mater. Sci.* **27** (1992) 1409.
17. I. M. ROBINSON, M. ZAKIKHANI, R. J. DAY and R. J. YOUNG, *J. Mater. Sci. Lett.* **6** (1987) 1212.

18. R. J. YOUNG, D. LU, R. J. DAY, W. F. KNOFF and H. A. DAVIS, *J. Mater. Sci.* **27** (1992) 5431.
19. W. F. WONG and R. J. YOUNG, *ibid.* **29** (1994) 510.
20. R. J. YOUNG, C. GALIOTIS, I. M. ROBINSON and D. N. BATCHELDER, *ibid.* **22** (1987) 3642.
21. M. C. ANDREWS and R. J. YOUNG, *J. Raman Spectrosc.* **24** (1993) 539.
22. R. J. DAY, X. HU and R. J. YOUNG, *Compos. Sci. Technol.* **48** (1993) 255.
23. N. MELANITIS, C. GALIOTIS, P. L. TETLOW and C. K. L. DAVIES, *J. Compos. Mater.* **26** (1992) 574.
24. H. L. COX, *Br. J. Appl. Phys.* **3** (1952) 72.
25. L. B. GRESZCZUK, in "Interfaces in Composites", ASTM STP 452 (American Society for Testing and Materials, Philadelphia, PA, 1969) p. 42.
26. P. LAWRENCE, *J. Mater. Sci.* **7** (1972) 1.
27. P. S. CHUA and M. R. PIGGOTT, *Compos. Sci. Technol.* **22** (1985) 33.
28. *Idem, ibid.* **22** (1985) 107.
29. *Idem, ibid.* **22** (1985) 185.
30. *Idem, ibid.* **22** (1985) 245.
31. A. KELLY and N. H. MÁĆMILLAN, "Strong Solids", 3rd edn (Clarendon Press, Oxford, 1986).
32. J. BOWYER and M. G. BADER, *J. Mater. Sci.* **7** (1972) 1315.
33. R. K. MITTAL and V. B. GUPTA, *ibid.* **17** (1982) 3179.
34. A. KELLY and W. R. TYSON, *J. Mech. Phys. Solids* **13** (1965) 329.
35. P. J. HERRERA-FRANCO and L.T. DRZAL, *Composites* **23** (1992) 2.
36. M. R. PIGGOTT, in "Interfacial Phenomena in Composite Materials '91", edited by I. Verpoest and F. R. Jones (Butterworth-Heinemann, Oxford, 1991) p. 2.
37. W. R. TYSON and G. DAVIS, *Br. J. Appl. Phys.* **10** (1963) 199.
38. D. M. SCHUSTER and E. SCALA, *Am. Inst. Aero. Astro. J.* **6** (1978) 527.
39. Y. HUANG and R. J. YOUNG, *Carbon*, in press.
40. L. S. PENN, F. BYSTRY, W. CARP and S. LEE, in "Molecular Characterisation of Interfaces", edited by H. Ishida and G. Kumar (Plenum, New York, 1985) pp. 93.
41. J. P. FAVRE and J. PERRIN, *J. Mater. Sci.* **7** (1972) 1113.
42. J. P. FAVRE and M. C. MÉRIENNE, *J. Adhes. Adhes.* **1** (1981) 311.
43. P. MARSHALL and J. PRICE, *Composites* **22** (1991) 53.
44. R. VIDAMO and D. B. FISCHBACH, *J. Am. Ceram. Soc.* **61** (1980) 13.
45. H. SAKATA, M. DRESSELHAUS and M. ENDO, in "Proceedings of the 18th Carbon Conference" Worcester Polytechnic Institute, Worcester MA. 1987 (Worcester Polytechnic Institute) 18.
46. J.-B. DONNET and R. C. BANSAL, "Carbon Fibres" (Marcel Dekker, New York, Basel, 1984).
47. C. GALIOTIS and D. N. BATCHELDER, *J. Mater. Sci. Lett.* **7** (1988) 545.
48. G. DÉSARMOT and J. P. FAVRE, *Compos. Sci. Technol*, **42** (1991) 151.
49. M. R. PIGGOTT and D. ANDISON, *J. Reinf. Plast. Compos.* **6** (1987) 290.
50. D. HULL, "An Introduction to Composite Materials" (Cambridge University Press, Cambridge, 1981).

Received 22 August
and accepted 4 October 1994